

Importance of using ensemble estimated background error covariances for the quality of atmospheric ozone analyses

S. Massart,^{a*} A. Piacentini^a and O. Pannekoucke^b

^aCERFACS/CNRS, URA 1875, Toulouse, France

^bMétéo-France/CNRS, CNRM/GAME URA 1357, Toulouse, France

*Correspondence to: S. Massart, CERFACS, 42 avenue Gaspard de Coriolis, 31057 Toulouse Cedex 01, France.

E-mail: massart@cerfacs.fr

An ensemble method combined with a four-dimensional variational data assimilation system is used to provide monthly estimates of the background error covariance matrix for global stratospheric and upper tropospheric ozone for the year 2008. The system is composed of the Mocage chemical transport model and the Valentina assimilation system. The ensemble was obtained from parallel analyses of perturbed data from the Microwave Limb Sounder (MLS) instrument. The monthly estimates of background error covariances have then been introduced in the assimilation suite. To assess the separate contribution of each of its components, a number of analyses were realized, using only some estimated components of the background error covariances and a basic model for the others. The evaluation is realized by comparing the analyses with independent ozone profiles (from ozonesondes) and total ozone columns (from the Ozone Monitoring Instrument). It demonstrates that using the estimated statistics compared to basic models for the background error covariance matrix globally slightly improves the analysis quality; however, using the estimated statistics more largely improves the analysis quality for special situations encountered in April and October. In these situations, the most important parameter for the analysis quality is the use of estimated correlations. Copyright © 2011 Royal Meteorological Society

Key Words: data assimilation; atmospheric chemistry; background error covariance matrix

Received 3 March 2011; Revised 5 September 2011; Accepted 18 October 2011; Published online in Wiley Online Library 28 November 2011

Citation: Massart S, Piacentini A, Pannekoucke O. 2012. Importance of using ensemble estimated background error covariances for the quality of atmospheric ozone analyses. *Q. J. R. Meteorol. Soc.* **138**: 889–905. DOI:10.1002/qj.971

1. Introduction

The background error covariance matrix (BECM) is a key component of any assimilation system (Kalnay, 2003). It represents the statistical error of the background state with respect to the true state. The background state usually comes from a model forecast and its statistics can therefore be evaluated, but the true state is by definition unknown. The aim of the assimilation process is to approximate it using a numerical model, a background state and some observations. BECM accounts for the background error variance (or standard deviation) and for the background error correlation. These two components can be assessed

separately. The background error variance has to be compared to the observation error variance in order to evaluate their relative weight in the analysis produced by the assimilation process. The background error correlation combines spatial correlation and correlation between the different model variables. The spatial correlation spreads the information brought in by observations at their locations to the neighbouring grid points. It is usually expressed through the introduction of length-scales. Correlation between the variables transfers the information to other model variables, if these are physically related to the variable directly linked to the measurements and if the physical relations between the variables are represented in the model.

Evaluation of the BECM is an essential challenge as it conditions the assimilation analysis. Nevertheless, the BECM comprises statistical information that is not directly obtainable since the true state is unknown. To get around this problem, in atmospheric chemistry quite often only the variance part of the BECM is considered. When the correlation part of the BECM is considered, its model is generally basic. As an example, in the ASSET intercomparison of ozone analyses (Geer *et al.*, 2006) only three of five systems based on chemical transport models (CTMs) accounted for background error horizontal correlations: the Royal Netherlands Meteorological Institute (KNMI) system (which operates the TM5 CTM) and the Mocage-Palm (later referred to as Valentina) system, both with a constant length-scale; and MIMOSA for which the correlations were flow dependent and specified in terms of distances and of the potential vorticity field. Moreover, the Kalman filter approach used in the MIMOSA and KNMI–TM5 systems allowed advection of background error variances. Since then, except for the recent work of Schwinger and Elbern (2010), evaluation of the BECM for global atmospheric chemistry has not been the object of thorough investigations. Previous work concerning the BECM is mainly focused on its formulation for atmospheric applications (Bannister 2008a, 2008b) or atmospheric chemistry (Pannekouce and Massart, 2008; Elbern *et al.*, 2010).

Meanwhile, in meteorology background (and analysis) errors have been successfully assessed using ensemble data assimilation systems. Exploitation in a cycled assimilation system could produce an estimate of a flow-dependent BECM. The ensemble approach is not restrained to Kalman filter methodologies. Lorenc (2003) and Buehner (2005) illustrated how an ensemble-estimate BECM can be estimated within a variational assimilation system. Useful information could statistically be extracted from an adequately perturbed ensemble data assimilation system (Belo Pereira and Berre, 2006). The use of ensembles in combination with a variational assimilation scheme is relatively unexplored in atmospheric chemistry data assimilation. The main purpose of this study is to investigate the potential of an ensemble of atmospheric ozone analyses to provide useful flow-dependent estimates of the background error variance and correlations, in a four-dimensional variational assimilation suite. Moreover, we assess the sensitivity of the analyses to the choice of fixed or estimated variance and correlations. Our results are based on stratospheric and upper tropospheric ozone analyses realized during a one-year period starting from January 2008.

2. Global atmospheric ozone analysis

In this study, the Météo-France Mocage (MOdèle de Chimie Atmosphérique Grande Échelle) CTM is used as the forecast model that produces global atmospheric ozone concentrations from the surface to the lower mesosphere. It is combined with stratospheric and upper tropospheric ozone profile measurements from the Microwave Limb Sounder (MLS) instrument, using a four-dimensional variational (4D-Var) assimilation scheme. The 4D-Var scheme is implemented within Valentina, a modular variational data assimilation suite developed at CERFACS.

2.1. Numerical ozone forecast

Mocage is a three-dimensional CTM that calculates the evolution of the atmosphere's composition in accordance with dynamical, physical and chemical processes (Peuch *et al.*, 1999). It covers the planetary boundary layer, the free troposphere, the stratosphere and a part of the mesosphere. It provides a number of optional configurations with varying domain geometries and resolutions, as well as chemical and physical parametrization packages.

Mocage is currently used for several applications. Using its nested domains, it routinely provides the Météo-France operational chemical weather forecasts (Dufour *et al.*, 2004). In its global version, it has been recently validated using a large number of measurements during the Intercontinental Transport of Ozone and Precursors (ICARTT/ITOP) campaign (Bousserez *et al.*, 2007). Its climate version has also been validated over several years by Teyssède *et al.* (2007). Being a part of the Valentina assimilation system, the global version of Mocage was widely used for assimilation studies, with recent examples in Claeysman *et al.* (2010), El Amraoui *et al.* (2010), Massart *et al.* (2009) and Semane *et al.* (2009).

In this study, we used the $2^\circ \times 2^\circ$ global version of Mocage, with 60 vertical levels (from the surface up to 0.1 hPa). As a CTM, its advection scheme depends upon dynamical fields. The meteorological forcing fields are the analyses provided by the operational European Centre for Medium-Range Weather Forecasts (ECMWF) numerical weather prediction model.

We propose in the following to estimate the BECM with an ensemble of assimilations. This involves a large number of CTM simulations. Since the chemical component of a CTM usually accounts for most of the computational cost, a fast chemical scheme is essential for this study. We therefore adopted the linear ozone parametrization developed by Cariolle and Teyssède (2007) in its latest version. Even though much cheaper in terms of computational time, when combined with the assimilation process, this scheme provides analyses close to the results of a more complete chemical scheme within the vertical range where assimilated data are available (Geer *et al.*, 2006).

2.2. Ozone analysis

In this study, we produced atmospheric ozone analyses from MLS data with the Valentina assimilation system coupled with Mocage using CERFACS Palm (Projet d'Assimilation par Logiciel Multi-méthodes) software. Valentina is based on the Mocage-Palm system previously developed jointly by CERFACS and Météo-France in the framework of the FP5 European project ASSET (Lahoz *et al.*, 2007). Since ASSET, however, Mocage-Palm was extended with the support of the Ether Centre for Atmospheric Chemistry Products and Services and became Valentina (Massart *et al.*, 2007, 2009).

2.2.1. Assimilation method

Valentina used to work with the FGAT (first guess at appropriate time) variant of the three-dimensional variational method (3D-Var). We found in Massart *et al.* (2010), however, that this method does not localize well (in space) the increment when the dynamics are rapid in the stratosphere, even with an assimilation window size

of 3 hours. Reducing the size of the assimilation window increases the computational cost. As we wanted a reasonable cost to produce an ensemble of assimilations, we chose to implement a four-dimensional variational method. The 4D-Var avoids the 3D-FGAT problem of increment localization.

Mocage is a chemical transport model. Therefore the 4D-Var method requires linear tangent and adjoint models of the transport and chemical components. Only the transport component is modelled in the assimilation process and it is already linear. Nevertheless, Mocage uses a semi-Lagrangian scheme to model the transport. This involves computing some interpolation coefficients and then performing the interpolation with these coefficients. Computation of the interpolation coefficients consumes most of the computational cost. However, these coefficients are computed during the model forecast and stored for assimilation. The linear tangent and adjoint models of the transport model thus perform only interpolations using the previously stored coefficients. These interpolations have a low computational cost compared to the full transport model. Therefore, with the 12 hours assimilation window we use in this study, the 4D-Var takes only slightly longer than the previous 3D-FGAT configuration with a 3-hour window when we limit to 100 the number of iterations of the minimization process for each assimilation window.

2.2.2. Background error variances

The background error covariance \mathbf{B} matrix is split into a correlation matrix \mathbf{C} and a diagonal matrix $\mathbf{\Sigma}$ filled with the background error standard deviation:

$$\mathbf{B} = \mathbf{\Sigma} \mathbf{C} \mathbf{\Sigma}. \quad (1)$$

The $\mathbf{\Sigma}$ matrix of Eq. (1) represents the background error standard deviation of the assimilated chemical species in each grid point of the model. This matrix has to be specified for each assimilation experiment. Note that a basic model for the standard deviation is to choose it to be proportional to the background state.

2.2.3. Correlation model

Building a correlation matrix is not a trivial task since it has to satisfy several constraints, such as being a positive-definite symmetric matrix. Moreover, the size of this matrix is the square of the size of the control vector. As we control only one species, the size of the control vector is equal to the number of the CTM grid points, which is already elevated. Adding other species in the control vector may dramatically increase the size of \mathbf{C} to a point where building the matrix in the computer memory could become impossible. For these reasons, we chose to follow Weaver and Courtier's (2001) approach. Our background error correlation operators are built upon the product of \mathbf{L} by \mathbf{W}^{-1} , where \mathbf{L} corresponds to the discrete operator resulting from a time integration of a diffusion equation and \mathbf{W} is a diagonal matrix of local area elements (length of the cells for one-dimensional grids, and area of the cells for two-dimensional grids). The time integration of a diffusion equation allows one to produce covariance functions. The methodology then consists in fixing the time integration and in building the local diffusion tensor \mathbf{v} that produces the desired correlations when the diffusion is applied to a field. As the product

\mathbf{LW}^{-1} generates covariance functions, it has to be scaled by a diagonal normalization matrix $\mathbf{\Lambda}^2$ to obtain correlation functions. We then use the fact that $\mathbf{LW}^{-1} = \mathbf{L}^{1/2} \mathbf{W}^{-1} \mathbf{L}^{T/2}$, where $\mathbf{L}^{T/2}$ is the adjoint operator of $\mathbf{L}^{1/2}$, the square root of \mathbf{L} (Weaver and Courtier, 2001). The correlation operator is thus formulated as

$$\mathbf{C} = (\mathbf{\Lambda} \mathbf{L}^{1/2} \mathbf{W}^{-1/2}) (\mathbf{\Lambda} \mathbf{L}^{1/2} \mathbf{W}^{-1/2})^T, \quad (2)$$

which provides the required symmetry.

To simplify the computation of this product, the hypothesis of horizontal-vertical correlation separability was chosen. This choice could be justified assuming the correlations are mainly controlled by the transport in a CTM. The transport is well decomposed in a horizontal component and a vertical component on the sigma-hybrid vertical coordinate of the model. As a consequence, the size of an error structure on the horizontal may not have an impact on the vertical distribution of this structure. The correlation was thus divided into a horizontal (subscript h) and a vertical (subscript v) operator, $\mathbf{C} = (\mathbf{C}_h^{1/2} \mathbf{C}_v^{1/2}) (\mathbf{C}_h^{1/2} \mathbf{C}_v^{1/2})^T$.

2.2.4. Background error vertical correlations

The vertical correlation is decomposed as the product $\mathbf{C}_v^{1/2} \mathbf{C}_v^{T/2}$, where $\mathbf{C}_v^{1/2} = \mathbf{\Lambda}_v \mathbf{L}_v^{1/2} \mathbf{W}_v^{-1/2}$. The vertical coordinate z is expressed in the natural logarithm of the pressure and \mathbf{W}_v represents the length of the cells in this coordinate system. \mathbf{L}_v is computed with an implicit time integration scheme of the one-dimensional diffusion equation. The local diffusion tensor \mathbf{v}_v is filled with half of the square of the space-dependent length-scale $L_z(z)$ as described by Daley (1991). The local normalization is based on the Gaussian normalization factor $\mathbf{\Lambda}_v(z) = \sqrt{2\pi} L_z(z)$.

The diffusion-based approach presents some limitations. First, the diffusion equation has to be solved with a time step that tends toward zero to ensure a Gaussian shape. Second, this approach is quite simple in an infinite or periodic domain but has to be adapted in the case of boundary conditions. These limitations were explored by Mirouze and Weaver (2010). The authors detail the correlation function obtained by the solution of the one-dimensional diffusion equation using an implicit time integration, as a function of the number of time steps M (i.e. the inverse of the time step length, the time integration being fixed to one in units of the chosen time unit). The local diffusion tensor \mathbf{v}_v has to be divided by $\sqrt{1 - 3/M}$ and the local normalization $\mathbf{\Lambda}_v$ by $\sqrt{1 - 1/M}$. They also propose a methodology to treat boundary conditions. This methodology was here derived and the vertical correlation is built by solving two one-dimensional diffusion equations: one with a Dirichlet boundary condition and the other with a Neumann one, using an implicit time integration. Our adaptation of the Mirouze and Weaver (2010) methodology greatly improves the treatment near boundaries, but not at the boundaries themselves. Nevertheless, the uppermost data value we used (see section 2.3) is located at a distance of 3 grid points from the top of the model vertical grid. The lowermost data value is located near the middle of the vertical grid.

2.2.5. Background error horizontal correlations

Like the vertical, the horizontal correlation is decomposed as the product $\mathbf{C}_h^{1/2} \mathbf{C}_h^{T/2}$, where $\mathbf{C}_h^{1/2} = \mathbf{\Lambda}_h \mathbf{L}_h^{1/2} \mathbf{W}_h^{-1/2}$. \mathbf{C}_h is

applied for each grid level on the two-dimensional spherical domain with the coordinates (λ, θ) . The metric Λ_h is then filled with the area of the grid cells.

With a homogeneous and isotropic correlation length-scale all over the globe, L_h corresponds to the integration of a diffusion equation on the sphere with a constant diffusion coefficient. In that case, we chose to compute L_h in the spherical harmonics space. This leads to a simple and faster computation. Moreover, Λ_h and \mathbf{W}_h are both reduced to a single scalar.

When the correlation length-scales are not homogeneous, a local diffusion tensor $\mathbf{v}(\lambda, \theta)$ has to be used. If L_λ (L_θ) designates the local one-dimensional differential length-scale along the direction λ (θ) Pannekoucke and Massart (2008) introduce the tensor

$$\mathbf{\Gamma}^{-1}(\lambda, \theta) = \begin{pmatrix} \frac{1}{L_\lambda^2(\lambda, \theta)} & \frac{1}{L_{\lambda\theta}(\lambda, \theta)} \\ \frac{1}{L_{\lambda\theta}(\lambda, \theta)} & \frac{1}{L_\theta^2(\lambda, \theta)} \end{pmatrix}. \quad (3)$$

The local diffusion tensor \mathbf{v} is related to $\mathbf{\Gamma}$ by $\mathbf{v}(\lambda, \theta) = \mathbf{\Gamma}(\lambda, \theta)/2$. $L_{\lambda\theta}$ allows one to represent the anisotropy, when the reference direction formed with the eigenvectors of the local diffusion tensor \mathbf{v} is rotated compared to the classical east–west and north–south directions. Such an anisotropy is not yet represented in our system ($L_{\lambda\theta} = 0$). Nevertheless, anisotropy appears on the sphere with heterogeneity, i.e. when the two length-scales L_λ and L_θ differ.

The L_h is again modelled using an implicit time integration scheme, based on the above-described local diffusion tensor \mathbf{v} . The implicit time integration allows removal of all stability limitations on the time step (as required in the explicit case), especially over the polar regions, where the grid cells are smaller than those of the equatorial region. The drawback is a reduced precision. Nevertheless, even with a few time steps, the implicit scheme has a sufficient precision and has an extremely low cost compared to an explicit scheme.

One main difficulty when using a local diffusion tensor with the diffusion equation to model the local correlations is to set the normalization matrix Λ_h (which ensures transformation of the covariances generated by $L_h \mathbf{W}_h^{-1}$ to correlations). We choose here the approximation proposed by Pannekoucke and Massart (2008) that links the local normalization to the local diffusion tensor by

$$\Lambda(\lambda, \theta) = \sqrt{2\pi |\mathbf{\Gamma}(\lambda, \theta)|^{1/2}}, \quad (4)$$

where $|\mathbf{\Gamma}|$ is the determinant of $\mathbf{\Gamma}$.

2.2.6. *A posteriori diagnostics*

The innovation vector $\mathbf{d} = \mathbf{y}^o - \mathbf{H}\mathbf{x}^b$ computes the difference between the observation \mathbf{y}^o and the background \mathbf{x}^b projected in the observation space by the observation operator \mathbf{H} , which is assumed linear hereafter. It can also be expressed as a function of the observation error ϵ^o and the background error ϵ^b , so $\mathbf{d} = \epsilon^o - \mathbf{H}\epsilon^b$. When the observation error and the background error are not correlated, the mathematical expectation \mathbb{E} of $\mathbf{d}\mathbf{d}^T$ is a function of the BECM, the \mathbf{R} observation error covariance matrix (OECM) and the observation operator:

$$\mathbb{E}[\mathbf{d}\mathbf{d}^T] = \mathbf{R} + \mathbf{H}\mathbf{B}\mathbf{H}^T. \quad (5)$$

Equation (5) is not useful in this form as it mixes both the BECM and the OECM. However, multiplying on the left both sides by $\mathbf{I} - \mathbf{H}\mathbf{K}$, where \mathbf{I} is the identity matrix and $\mathbf{K} = \mathbf{B}\mathbf{H}^T (\mathbf{H}\mathbf{B}\mathbf{H}^T + \mathbf{R})^{-1}$ is the gain matrix, leads to

$$\mathbb{E}[(\mathbf{I} - \mathbf{H}\mathbf{K})\mathbf{d}\mathbf{d}^T] = \mathbf{R}. \quad (6)$$

According to the expression of \mathbf{d} and \mathbf{K} , one can demonstrate that $(\mathbf{I} - \mathbf{H}\mathbf{K})\mathbf{d} = \mathbf{y}^o - \mathbf{H}\mathbf{x}^a$, where \mathbf{x}^a is the analysis. That implies for Eq. (6)

$$\mathbb{E}[(\mathbf{y}^o - \mathbf{H}\mathbf{x}^a)\mathbf{d}^T] = \mathbf{R}. \quad (7)$$

This means that computing an analysis with an appropriate OECM must satisfy Eq. (7). If this relation is not satisfied, the OECM can be updated using the left-hand side of Eq. (7). However, this requires the computation of the mathematical expectation over several realisations. A useful way of using Eq. (7) is to assume a good shape of the OECM but a wrong amplitude. A multiplicative correction factor s_o^2 can then be computed and applied to the used OECM \mathbf{R} . It is computed with a comparison of the trace of the two matrices of Eq. (7):

$$s_o^2 = \frac{\mathbb{E}[\mathbf{d}^T (\mathbf{y}^o - \mathbf{H}\mathbf{x}^a)]}{\text{Trace}(\mathbf{R})}, \quad (8)$$

as $\text{Trace}(\mathbb{E}[(\mathbf{y}^o - \mathbf{H}\mathbf{x}^a)\mathbf{d}^T]) = \mathbb{E}[\mathbf{d}^T (\mathbf{y}^o - \mathbf{H}\mathbf{x}^a)]$. An assimilation experiment can then be run using the updated OECM $s_o^2 \mathbf{R}$. In Valentina, we compute s_o^2 according to Eq. (8) but using several time-consecutive assimilation experiments for computing the mathematical expectation. Moreover, a similar s_b^2 coefficient for the BECM can be expressed. It requires the computation of $\text{Trace}(\mathbf{H}\mathbf{B}\mathbf{H}^T)$, which is not available in our system. We then compute s_b^2 in order to impose that twice the minimum of the cost function is equal to the number of observations over several time-consecutive assimilation experiments (Talagrand, 2003). Assume that $J^b(\mathbf{x}^a)$ and $J^o(\mathbf{x}^a)$ are respectively the background and the observation terms of the cost function at its minimum. Given s_o^2 by Eq. (8), in the case of one assimilation window, we search s_b^2 such as $s_b^{-2} J^b(\mathbf{x}^a) + s_o^{-2} J^o(\mathbf{x}^a) = p/2$, where p is the number of observations within the assimilation window. This leads to calculation of s_b^2 , with

$$s_b^2 = \frac{J^b(\mathbf{x}^a)}{p/2 - s_o^{-2} J^o}, \quad (9)$$

which can easily be extended for several time-consecutive assimilation experiments. When the right-hand side of Eq. (9) is negative, we choose to set s_b^2 to the value obtained from the previous assimilation windows.

2.3. *Ozone observations*

The ozone analysis combines Mocale forecasts and data provided by the MLS instrument. This instrument has been flying onboard the Aura satellite in a sun-synchronous polar orbit since August 2004. Vertical profiles of several atmospheric parameters are retrieved from the millimetre and sub-millimetre thermal emission measured at the atmospheric limb (Waters *et al.*, 2006).

The MLS ozone product is a suitable dataset to analyse atmospheric ozone. It provides about 3500 profiles per day with a nearly global latitude coverage between 82°S and 82°N. Moreover, it provides data both in the stratosphere and the upper troposphere–lower stratosphere (UTLS). For our study we used the v2.2 version of the MLS ozone product.

Two successive MLS scans are separated by 24.7 s and 1.5°. This horizontal resolution is higher than the model horizontal grid of $2^\circ \times 2^\circ$. We therefore computed the average profile of all the profiles measured within a minute in the same model grid cell. This process reduces the number of profiles to about 2000 per day. A screening was also applied according to the recommendations of Froidevaux *et al.* (2008) and Livesey *et al.* (2008), i.e. the same screening we previously used in Massart *et al.* (2009). As they also recommend for ozone retrievals, we restricted the data selection to the pressure range from 215 to 0.5 hPa. This represents measurements at 16 pressure levels, with four of them located in the UTLS. Notwithstanding, the MLS ozone product has its highest error in the UTLS, with values from 5% to 100% below 100 hPa and from 2% to 30% at 100 hPa.

The observation error variances are computed using the square of the given standard deviations of the MLS observation error. This formulation only includes instrumental error and misses the representativeness error. The representativeness error is then introduced with the s_o coefficient of Eq. (8), the square of which is applied to the OECM. The value of s_o is adjusted for each assimilation window, but for the assimilation experiments we ran (see sections 3 and 4 for details), the average value is 1.69 ± 0.1 . Figure 1 shows the average standard deviation of the observation error as the MLS instrumental error multiplied by the 1.69 factor.

The random observation error of one level over a profile is assumed to be independent of the random observation error of the other levels along the same profile and of levels over other profiles. This means that there is no spatial or temporal correlation of the observation error. The off-diagonal terms of the observation error covariance matrix are then equal to zero. Moreover, Froidevaux *et al.* (2008) showed that the

averaging kernels' peaks are close to unity for the selected assimilated levels. This implies that we can use the MLS data without specifying the averaging kernels.

3. Estimated background error covariances

To set up the assimilation system with pertinent background error covariances, we chose to estimate them through an ensemble of assimilation analyses followed by an ensemble of forecasts. Forecast states being used as background states for the following analysis, statistics on the ensemble of forecasts allows estimation of the background error covariances as proposed by Belo Pereira and Berre (2006).

We performed an ensemble of ozone forecasts, analysing the MLS data within the configuration described above for a period of one year. The one-year period allows a sufficient number of statistical realizations to compute significant statistics. Both ozone background error variances and correlation length-scales were estimated from the ensemble results.

3.1. Set-up of the ensemble

To create the ensemble of forecasts, five MLS datasets were built by adding to the retrieved measurements a random centred Gaussian noise with a standard deviation equal to the standard deviation of the MLS instrumental error. We carried five assimilation experiments with these five datasets for the one-year studied period. The only difference between the experiments is the assimilated dataset. In particular, the dynamical forcing is identical for all experiments.

As at this point, we had no pertinent information on the background errors and we had to make some assumptions on their covariances. Concerning the background error horizontal correlation, we chose a homogeneous length-scale in order to save computational time. We selected a trade-off value of 450 km for the homogeneous length-scale, which corresponds to the average of the zonal length-scale we found in Pannekoucke and Massart (2008).

Concerning the background error vertical correlation, we also chose a homogeneous length-scale. The value comes again from previous studies and was set to 0.22 (in units of the logarithm of pressure). The background error standard deviation was imposed as 15% of the background field. It therefore varies in space and time.

Fixing these values for the background error covariances model, we ran the five experiments in parallel from the same initial condition, i.e. 15 December 2007. As the five members shared the same initial condition, several cycles of forecasts are required to lose memory of the initial condition and to have a quasi-stationary spread of the ensemble. The study of the ensemble of forecasts thus began on 1 January 2008. With two forecasts per day and five members, we had an ensemble of ten elements per day, i.e. $\{\mathbf{x}_i^b(j)\}_{j=1,5}$ for the cycle i (at 0 UTC) and $\{\mathbf{x}_{i+1}^b(j)\}_{j=1,5}$ for the cycle $i+1$ (at 1200 UTC). As we needed a number of elements large enough to produce significant statistics, we decided to extract monthly statistics. For example, this allows computation of statistics on the 300 elements $\{\mathbf{x}_i^b(j)\}_{i=1,60,j=1,5}$ for a month composed of 30 days. With a preliminary sensitivity study, we estimated this number to be sufficiently large and we chose not to extend the number of elements by analysing periods longer than one month. This was driven by the fact

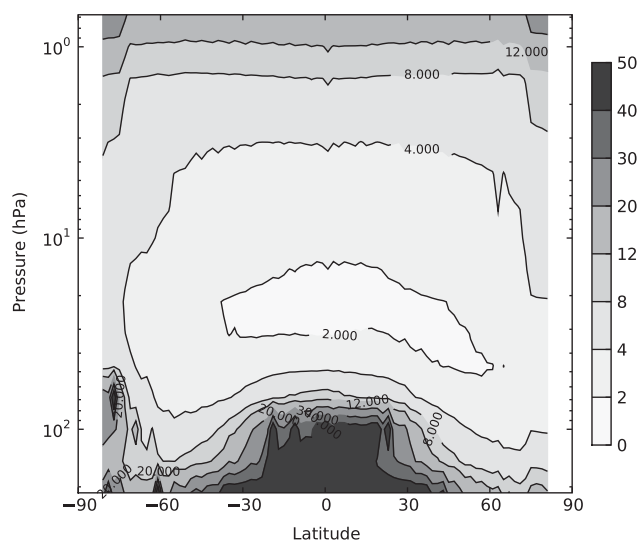


Figure 1. Zonal and time average of the standard deviation of the MLS ozone observation error (%) for the year 2008. The levels of the vertical coordinate are the 16 MLS pressure levels that are assimilated. The average is computed on a $2^\circ \times 2^\circ$ grid.

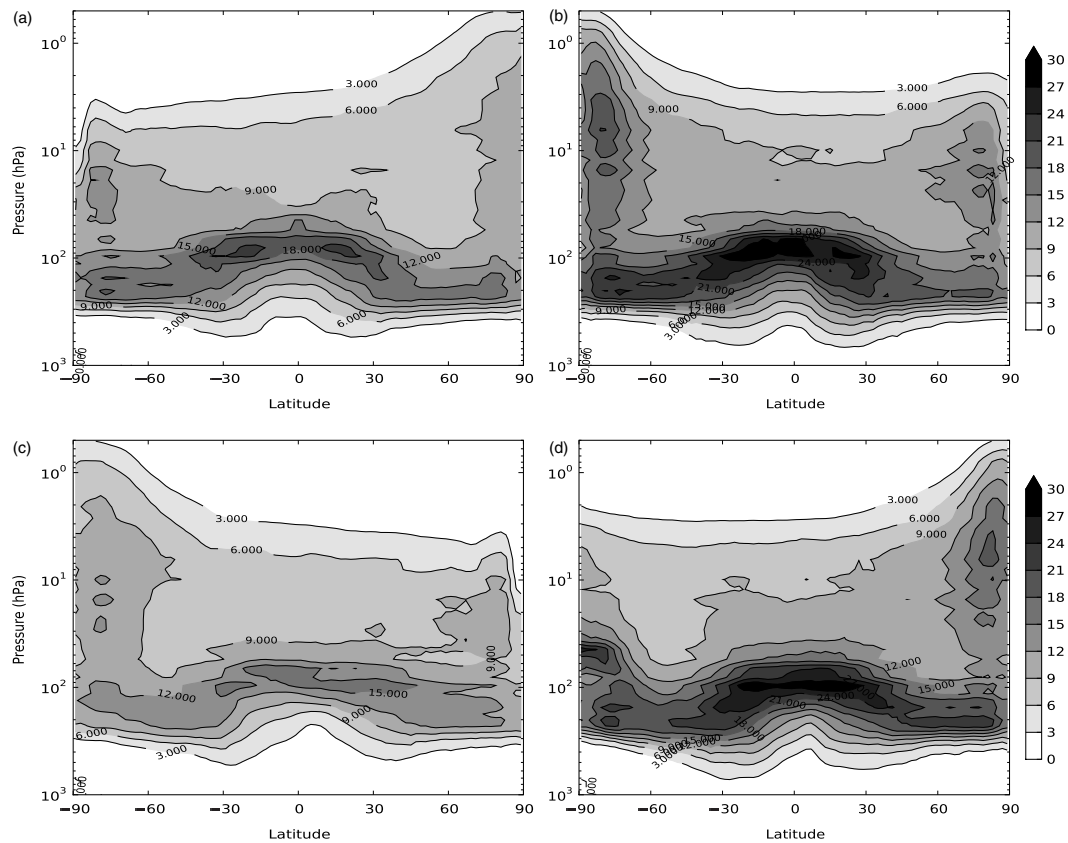


Figure 2. Zonal means of monthly estimated ozone standard deviations as percentage of the ozone field: (a) January, (b) April, (c) July and (d) October.

that we would keep some flow-dependent aspects, even if these aspects were already filtered by the monthly analysis.

For each assimilation cycle i , we computed the average background $\bar{\mathbf{x}}_i^b(j) = \frac{1}{5} \sum_{j=1}^5 \mathbf{x}_i^b(j)$, which was used as the reference to compute the background error. Monthly estimated statistics of the background error covariances were computed from the differences $\{\mathbf{x}_i^b(j) - \bar{\mathbf{x}}_i^b(j)\}_{i=1,2,d,j=1,5}$:

$$\mathbf{B} = \frac{1}{10d} \sum_{i=1}^{2d} \sum_{j=1}^5 (\mathbf{x}_i^b(j) - \bar{\mathbf{x}}_i^b(j)) (\mathbf{x}_i^b(j) - \bar{\mathbf{x}}_i^b(j))^T, \quad (10)$$

where d is the number of days in the month. The resulting statistics were decomposed in standard deviations, meridional, zonal and vertical correlation length-scales. As these monthly quantities represent a large number of results, we summarize hereafter their main characteristics.

Most results are displayed as zonal mean plots and latitude–longitude plots. The latitude–longitude plots are the simple vertical average over the pressure levels from 200 to 0.5 hPa. These pressure levels correspond approximately to the levels where MLS data are assimilated.

3.2. Estimated background error standard deviation

The ensemble of forecasts is obtained by perturbing only the assimilated observations and no other parameters such as the dynamical forcings. Nevertheless, we made the assumption that the data perturbation used to build the ensemble is sufficient to obtain the structures of the standard deviations, even if their amplitude is underestimated. This assumption was justified *a posteriori* as the shape of the estimated

standard deviations from Eq. (10) and shown in Figure 2 differs from the shape of the observation error (Figure 1). However, *a posteriori* diagnostics presented in section 2.2.6 suggest multiplying the estimated standard deviations by a factor s_b of about ten. All results shown here take into account this factor.

The background error standard deviation Σ presents a similar vertical shape over the 12 months of 2008. It is higher in the UTLS region, especially over the equatorial region with local maximum values between 20% and 30% of the ozone averaged concentration. These highest values of Σ are not equally distributed over latitude bands but are mainly localized over the Pacific Ocean and East Africa, as showed by the yearly averaged Σ on Figure 3.

The differences from one month to another are also localized in the north and south polar regions (respectively referred to hereafter as NPR and SPR). There, Σ stratospheric average is around 11% of the ozone concentration over the NPR and 13% over the SPR. During the polar night, however, Σ increases to values reaching 20% in a vertical region spanning the stratosphere. However, its values are distributed like a wave number 2 pattern over the NPR as two regions with a 90° phase shift hold the highest values (Figure 3).

3.3. Estimated background error vertical correlations

As previously stated in section 2.2.4, the vertical correlation of the background errors is represented by the local vertical length-scale L_z . For each grid point two vertical correlations are computed using the monthly ensemble of forecast errors from Eq. (10): ρ^+ with the upper pressure level localized at a distance δz^+ and ρ^- , with the lower pressure level localized

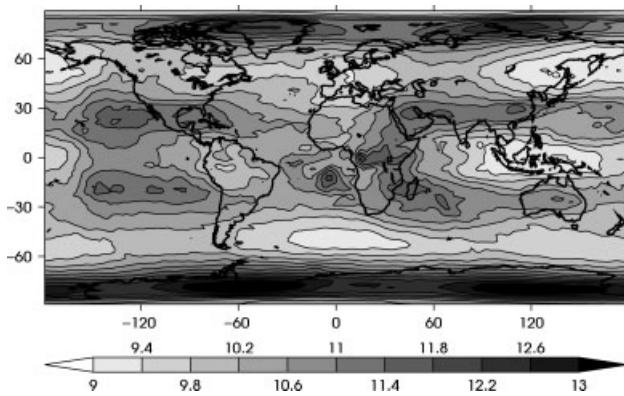


Figure 3. Yearly average of the monthly estimated ozone standard deviation, averaged over the 200–0.5 hPa levels, as percentage of the ozone concentration.

at a distance $\delta \mathbf{z}^-$. From these correlations, Pannekoucke *et al.* (2008) propose the following Gaussian-based length-scale formulation:

$$L_z^+(\mathbf{z}) = \frac{|\delta \mathbf{z}^+|}{\sqrt{-2 \ln \rho_z^+(\mathbf{z})}}, \quad (11a)$$

$$L_z^-(\mathbf{z}) = \frac{|\delta \mathbf{z}^-|}{\sqrt{-2 \ln \rho_z^-(\mathbf{z})}}. \quad (11b)$$

The horizontal-altitude-dependent length-scale L_z is then set as the average of these local L_z^+ and L_z^- values.

We found that L_z varies slightly with the altitude in the stratosphere (not shown). We therefore discuss only the 200–0.5 hPa level averages presented in Figure 4 for four months over 12. L_z has strong monthly variations. Nevertheless, its lowest values are always localized in a thin latitude band in the equatorial region. This band structure is more pronounced in January and October, with minimum values of 0.15 (in units of the logarithm of pressure, i.e. $\ln(\text{Pa})$). The highest L_z values are found in the vicinity of the band structure, with some maxima over 0.25 $\ln(\text{Pa})$ in July.

3.4. Estimated background error horizontal correlations

The horizontal correlations between the background errors are characterized by the zonal and the meridional length-scales, respectively L_λ and L_θ (see section 2.2.5). From each monthly ensemble of forecast errors, we computed from Eq. (10) and for each grid point (λ, θ) , the correlation $\rho_\lambda(\lambda, \theta)$ between the current grid point and its direct east neighbour localized at a distance $\delta\lambda(\lambda, \theta)$, and the correlation $\rho_\theta(\lambda, \theta)$ between the current grid point and its direct north neighbour localized at a distance $\delta\theta(\lambda, \theta)$. The zonal east length-scale $L_\lambda(\lambda, \theta)$ and the meridional north $L_\theta(\lambda, \theta)$ are then derived from the Gaussian-based formulation:

$$L_\lambda(\lambda, \theta) = \frac{|\delta\lambda(\lambda, \theta)|}{\sqrt{-2 \ln \rho_\lambda(\lambda, \theta)}}, \quad (12a)$$

$$L_\theta(\lambda, \theta) = \frac{|\delta\theta(\lambda, \theta)|}{\sqrt{-2 \ln \rho_\theta(\lambda, \theta)}}. \quad (12b)$$

Similar zonal and meridional length-scales are also computed using respectively the west and the south neighbour of each grid point. The zonal (meridional) length-scale is set as the average between the east (north) one and the west (south) one.

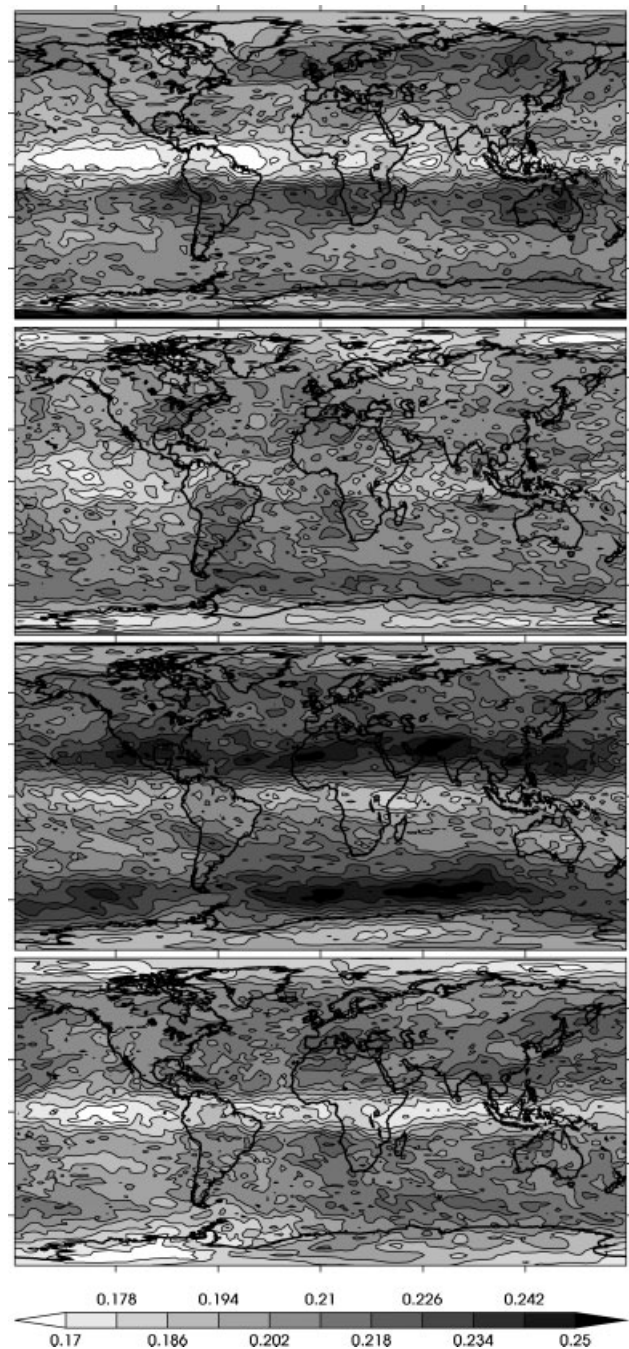


Figure 4. Monthly estimated ozone vertical length-scale L_z averaged over 200–0.5 hPa levels, in units of the natural logarithm of pressure. From top to bottom: January, April, July and October.

As for the estimated vertical length-scales, the estimated horizontal length-scales presents low variations within the pressure levels from 200 to 0.5 hPa. We then present only the vertical average between these levels.

3.4.1. Zonal length-scales

Analysis of the monthly estimated zonal length-scales L_λ as illustrated in Figure 5 reveals that they all have a quasi-sinusoidal variation with latitude. On average, their values increase from about 100 km over the South Pole to about 600 km at the Equator, and then they present a decrease to slightly lower than 100 km over the North Pole. L_λ thus has its lowest values of approximately 50 km, over the NPR

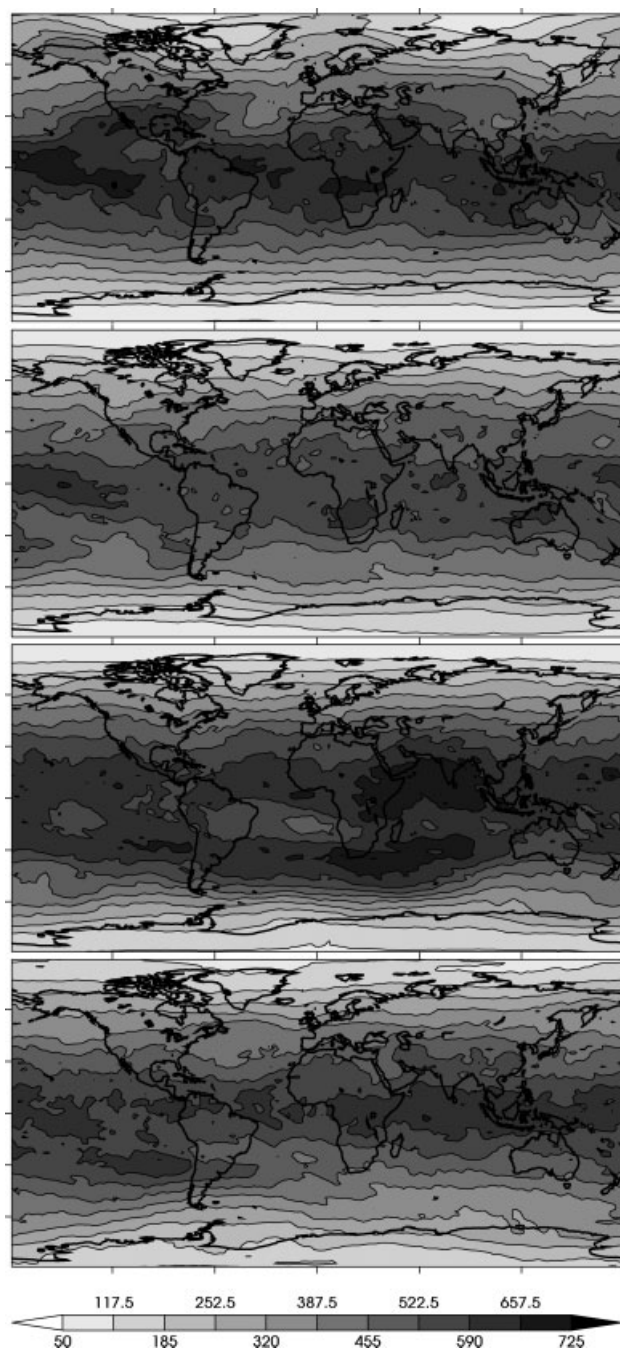


Figure 5. Same as Figure 4 except for the zonal length-scale (km).

and the SPR, and its highest values around 725 km over the equatorial region.

From May to July, the maximum is no longer located near the Equator but around 30°S. This can be related to the winter polar jet, which occurs during these months between 20 hPa and the mesosphere. The observed variability from one month to another in the tropical region is mainly linked to the variation of the L_λ values in the UTLS. This could be related to the significant variability of the dynamics in the UTLS. Another region where the variability remains important is the NPR. There, during the polar summer, the zonal length-scale does not vary much with longitude. However, during the polar winter, a wave number-2 pattern can be observed. A similar phenomenon is observed in the SPR but with a smaller amplitude.

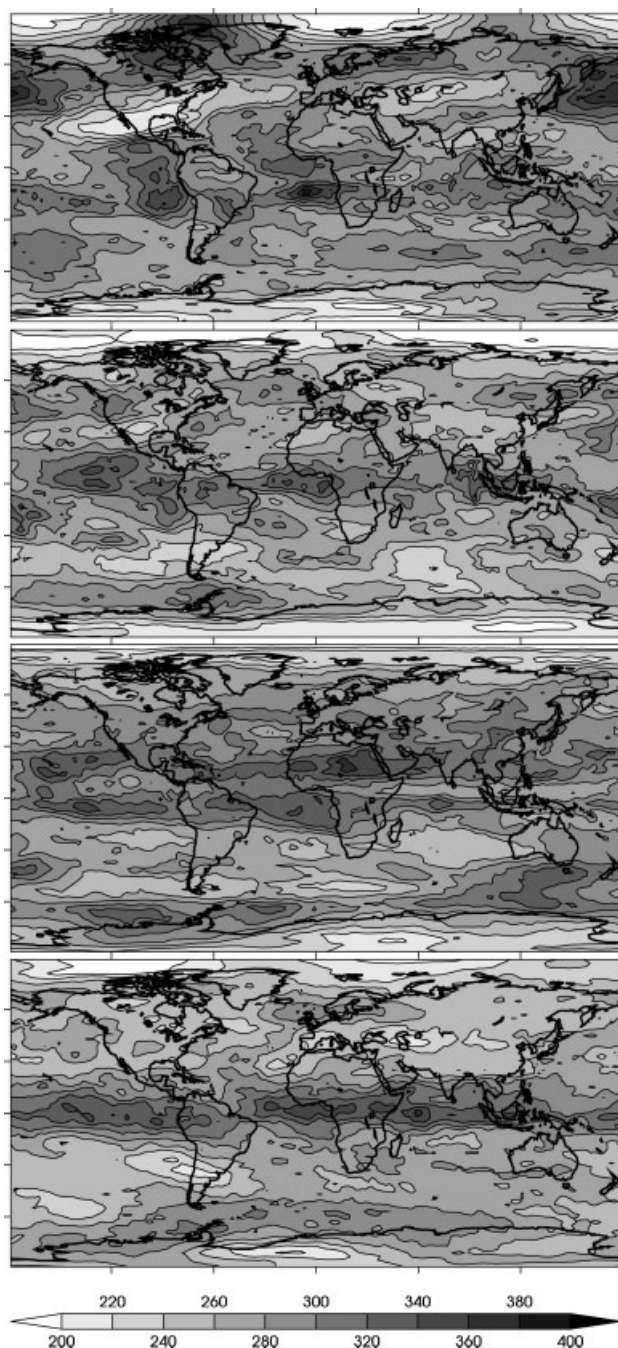


Figure 6. Same as Figure 4 except for the meridional length-scale (km).

3.4.2. Meridional length-scales

Figure 6 shows that the estimated meridional length-scales L_θ do not have the same sinusoidal variation with latitude as the zonal ones. Their lowest values are, however, found over the polar regions and their highest values are found over the equatorial region. On average, there is a thin latitude band around the Equator where the meridional length-scales have values of about 300 km, with the highest values found in the Pacific Ocean and especially in the Atlantic Ocean. In the equatorial part of the Atlantic Ocean, the highest values of L_θ are found from January to March.

Contrary to the zonal length-scales, the meridional ones vary with altitude (figure not shown). The largest values of L_θ (more than 300 km) are found in the UTLS, mainly between 60°S and 60°N. In the stratosphere, L_θ has lower

values, with an average of about 250 km, except in the NPR and SPR. There, L_θ has smaller values than elsewhere, with an average between 200 and 240 km for the SPR and between 180 and 220 km for the NPR. As for the zonal length-scales, L_θ does not vary much during the polar summer, but during the polar winter, particularly in the NPR, their values follow a wave number 2 pattern.

To sum up, in the tropical region the correlations between the background errors are mainly stretched in the zonal direction, with zonal length-scales twice as large as meridional ones. In the polar regions, the correlations are more isotropic and become stretched in the meridional direction over the poles. However, they may vary greatly spatially during the polar winter.

3.5. Impact on the estimations of the *a priori* assumptions on the BECM

The ensemble we used to estimate the background error covariances was built with *a priori* assumptions on the BECM, but when the *a priori* BECM is constant throughout the year, both the estimated background error variances and correlations show seasonal variations. They also show spatial variations that are not present in the *a priori* BECM. These variations are large compared to the constant values of the *a priori* BECM. This proves the low impact on the BECM estimation of the *a priori* BECM chosen to calculate the ensemble.

4. Background error covariance effects on ozone analysis

In this section, we investigate how moving from an ensemble-estimated BECM to a more basic model will affect the ozone analysis. As estimating the BECM is computationally expensive, we want to investigate which of its components is critical for obtaining good-quality analysis. Thus we first describe the methodology to evaluate the impact of the BECM configuration on the ozone analysis. The results are then presented for different layers of the atmosphere as well as for the atmospheric column.

4.1. Methodology

We originally planned to use the three-dimensional estimated horizontal length-scales, but, as presented in section 2.2.5, our numerical model for background error horizontal correlations integrates an implicit diffusion equation. This diffusion model is solved in a matricial form that requires the inversion of a huge matrix. It therefore represents an important part of the numerical cost of the assimilation. The cost is particularly high because the diffusion model has to be replicated for each level of the forecast model. To save computational time, we decided to impose the same L_λ and the same L_θ horizontal correlation length-scales for all the levels of the model. This allows us to invert only once the matrix of the implicit diffusion equation instead of 60 times in our case. This choice was justified by the fact that the ensemble estimate horizontal length-scales do not vary much for the pressure levels where MLS data are assimilated. The horizontal length-scales L_λ and L_θ used hereafter to model C_h are then equal to the vertical average over the pressure levels from 200 to 0.5 hPa of the values estimated from the ensemble.

For the vertical length-scale L_z as well as for the standard deviation Σ , we use the three-dimensional estimations, but to filter the noise in the statistics introduced by the monthly ensemble estimate we applied a binomial window filter. This transformation was applied to smooth the estimated fields with a width of five grid points in the horizontal plane and three grid points in the vertical direction.





In order to evaluate the impact of the BECM simplification on the analysis, we compare three assimilation experiments which differ only through the modelling of the BECM:

1. The first experiment, named FULL, uses the monthly estimated correlation length-scales and the monthly estimated background error standard deviation.
2. The second experiment, named PARTIAL, aims at evaluating the effect of not using the estimated standard deviation but only the monthly estimated correlation length-scales. The correlation length-scales used then all come from the ensemble estimate, and the standard deviation is set to a percentage of the background state. Besides this experiment, we performed another one using only the horizontal estimated correlation length-scales, the vertical one being constant. Using the estimated L_z has only a slight impact on the analysis, compared to the case where a constant L_z was used. We therefore decided to present only one of these two experiments, i.e. the one with the estimated L_z .
3. The third experiment, named BASIC, is of the same type as those used for building the ensemble (see section 3.1). The standard deviation of the background error is set to a percentage of the background state. The correlation length-scales of the background error are constant, with the same values as those used for the ensemble.

Experimental details are summarized in Table I. This table also presents the legend of each experiment used for the various plots presented hereafter.

The three aforementioned experiments were carried over the same period and assimilate the same MLS data as our ensemble runs used to estimate the BECM. Our strategy differs from that of Schwinger and Elbern (2010), who estimate the BECM on previous assimilation cycles and use it for the following cycles. Nevertheless, we aim to study the sensitivity of the analysis to the BECM components, the FULL experiment serving as a reference.

Table I. Characteristics of the experiments. The RAW experiment is a run without assimilation. The other assimilation experiments differ by the modelling of the BECM. See section 3 for the values of the estimated parameters.

Name	Σ	L_λ, L_θ	L_z	Legend
FULL	Estimated	Estimated	Estimated	
PARTIAL	15%	Estimated	Estimated	
BASIC	15%	450 km	0.22	
RAW	—	—	—	

4.2. Evaluation method

We evaluate the bias and the standard deviation (referred to as *STD*) of the analyses from the three previously described experiments, with respect to assimilated and independent data. Comparison with the MLS assimilated data helps in assessing the impact on the analysis of the model choice for the BECM correlation length-scales and standard deviation. Comparison with independent data helps to assess the ozone analysis quality for the different experiments. Comparison with a direct simulation referred to as *RAW*, produced with Mocage without any assimilation, is also performed.

The independent data chosen for the evaluation are profiles from ozonesondes and total ozone columns from the Ozone Monitoring Instrument (OMI; Levelt *et al.*, 2008). Ozone soundings are obtained from the World Ozone and Ultraviolet Radiation Data Centre (WOUDC, <http://www.woudc.org/>). They allow evaluation of the impact both in the troposphere and the lower stratosphere up to 5 hPa. OMI total ozone columns allow evaluation of the impact on the integrated vertical profile.

Average and *STD* of the differences between the datasets and the ozone analysis are computed both for every month and for the whole year. The average of the differences accounts for bias. For both comparison with MLS data and ozonesondes, the statistics are computed over the whole globe and for five latitude bands. The latitude bands are obtained by slicing the globe into 30° bands, except at the Equator, where the size of the band is 60°. Following Geer *et al.* (2006), the differences in the vertical profiles are normalized by a combination of the Logan (1999) tropospheric climatology with the Fortuin and Kelder (1998) stratospheric climatology. The bias and *STD* of the normalized differences are then expressed as percentages.

4.2.1. Comparison with MLS data

Comparison between the analysis and the assimilated MLS data is computed during the assimilation process, at the observation time and location. The comparison at the observation time is performed by a linear interpolation in time between two model states separated by 1 hour. Comparison at the observation location is obtained by doing a vertical linear interpolation and a bi-linear horizontal one.

For the whole year, global statistics are computed using more than seven hundred thousand data items. Data are regularly distributed over the months and the number of data for each of the five above described latitude bands is detailed in Table II.

4.2.2. Comparison with ozonesondes

Comparison between the assimilation products and ozonesondes is computed off-line. The comparison is realized at the observation location (with the same interpolation as for MLS data) but using the analysis at 1200 UTC. In this study, we use data from 17 locations mainly located in the latitude band from 30°N to 60°N as shown in Table III. These stations are mainly localized over Europe and provide the largest number of soundings (Table II). Most of the stations are equipped with electrochemical concentration cell (ECC) sondes. According to the laboratory experiment of Smit *et al.* (1998), the random variability error of the overall data is 10–15% in the

Table II. Number of MLS profiles and ozonesonde data per latitude band and for the whole domain, as used for the year 2008.

Lat. band	MLS	Sondes
90°S to 60°S	150 000	99
60°S to 30°S	106 000	68
30°S to 30°N	190 000	80
30°N to 60°N	106 000	496
60°N to 90°N	150 000	—
90°S to 90°N	7 000 000	743

Table III. Ozonesonde stations used for evaluation of ozone simulations. Stations are sorted by their latitude. Table headings ID, Station, Ctry, Lat. and Lon. represent the WOUDC station identification number, name, 3-character ISO country code, latitude and longitude respectively. See <http://www.woudc.org> for more details.

ID	Station	Ctry	Lat.	Lon.
323	Neumayer	ATA	70.7°S	8.3°W
101	Syowa	JPN	69.0°S	39.6°E
339	Ushuaia	ARG	54.9°S	68.3°W
254	Laverton	AUS	37.9°S	144.8°E
328	Ascension island	SHN	8.0°S	14.4°W
466	Maxaranguape	BRA	5.5°S	35.3°W
443	Sepang airport	MYS	2.7°N	101.7°E
336	Isfahan	IRN	32.5°N	51.7°E
107	Wallops island	USA	37.9°N	75.5°W
308	Barajas	ESP	40.5°N	3.6°W
156	Payerne	CHE	46.5°N	6.6°E
99	Hohenpeissenberg	DEU	47.8°N	11.0°E
242	Praha	CZE	50.0°N	14.4°E
318	Valentia observatory	IRL	51.9°N	10.2°W
316	De bilt	NLD	52.1°N	5.2°E
174	Lindenberg	DEU	52.2°N	14.1°E
221	Legionowo	POL	52.4°N	21.0°E

UTLS and near 5% in the middle stratosphere, where ozone concentrations are maximal.

4.2.3. Comparison with OMI data

To globally evaluate the analyses over the whole atmosphere, we also compared them to the total ozone columns measurements derived from OMI products. We used the retrievals obtained with the KNMI DOAS method (Veefkind *et al.*, 2006; data available from <http://www.temis.nl>). The OMI-DOAS total ozone columns showed a globally averaged agreement better than 2% with ground-based observations (Balis *et al.*, 2007). The data show no significant dependence on latitude except for the high latitudes of the Southern Hemisphere (SH), where there is a systematic overestimation of the total ozone value by 3–5%.

Owing to the high resolution of the OMI data, we averaged each OMI measurement scene (60 ground pixels) on a 2° × 2° horizontal grid (i.e. the model grid). For the one-year comparison period, this results in approximately 600

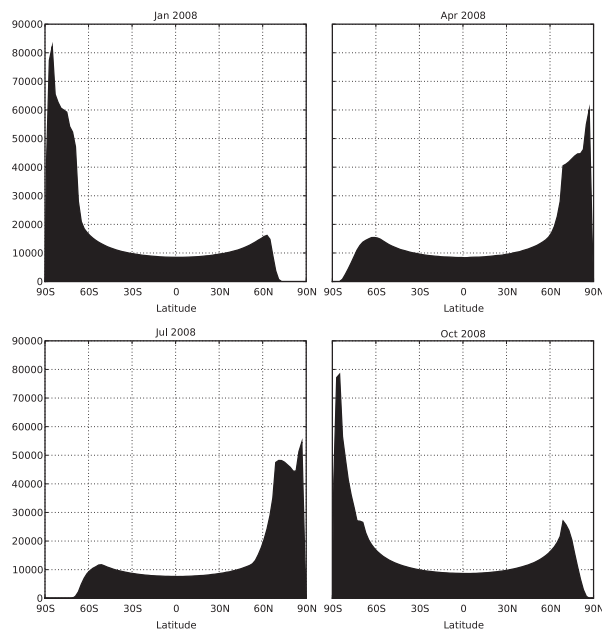


Figure 7. Sum over the longitude of the number of OMI measurements used for evaluation, for January, April, July and October 2008. The data are averaged by month and on a $2^\circ \times 2^\circ$ horizontal grid.

measurements at the Equator and 2000 measurements over the polar regions for each cell of the $2^\circ \times 2^\circ$ horizontal grid. Note that because OMI is an Ultraviolet–visible instrument, it does not provide any night-time measurement; this explains the variation in the number of high-latitude

measurements during the polar winter periods illustrated in Figure 7.

As for the ozonesondes, comparison between the assimilation products and OMI data is computed off-line. The comparison is also realized at the observation location (using the same interpolation as for other data) but using a linear time interpolation between the 12-hour step analyses. By construction, the comparison is realized on a $2^\circ \times 2^\circ$ grid and, contrary to ozonesondes, the differences are normalized by the observation measurement.

4.3. Evaluation of the FULL experiment

In the stratosphere, the observation error (Figure 1) is lower than the standard deviation of the background error estimated from the ensemble (Figure 2). Using this estimated Σ , the FULL analysis is thus mainly constrained by the observation, at the observation location. This is confirmed by Figure 8, in which the analysis shows a bias close to zero with respect to the assimilated MLS data, while the RAW model globally overestimates the ozone concentration, more particularly in the NPR and the SPR (where the bias ranges between 20% and 40%). Compared to ozonesondes, the FULL analysis also has a low stratospheric bias, and for all latitudes, as illustrated by Figure 9. The bias being lower than that from the RAW simulation demonstrates the ability of the assimilation of the MLS data to correct the stratospheric model bias. As expected by the assimilation of the MLS data, the stratospheric STD of the analysis compared to the MLS data is lower than the STD of the RAW simulation compared to the MLS data. Figure 8 shows that the FULL stratospheric

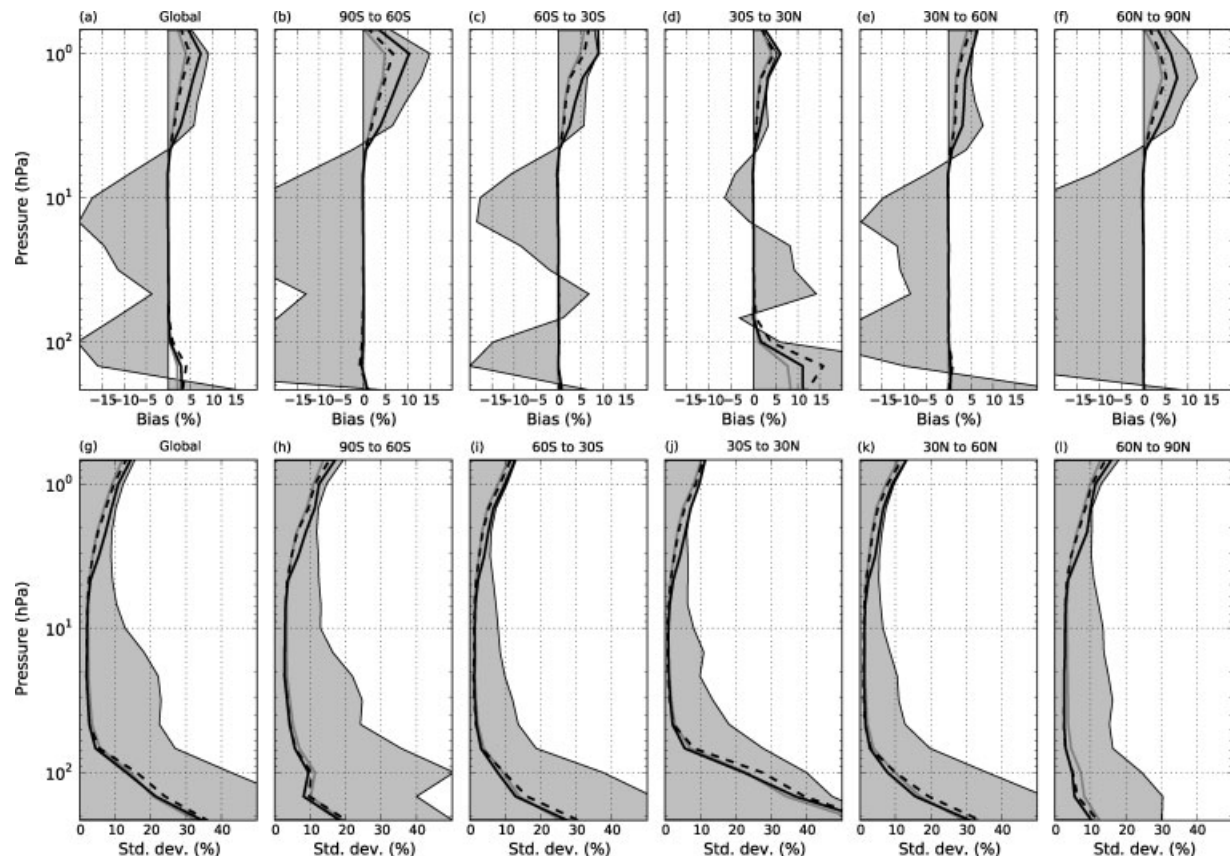


Figure 8. Mean (top) and standard deviation (bottom) of the difference (as percent of climatology) between MLS observations and the RAW model or the analyses, as a function of pressure level, and for different latitude bands. For the top panel, positive (negative) values stand for an underestimation (overestimation) of the RAW model or the analyses compared to the observations. See Table I for colour legend.

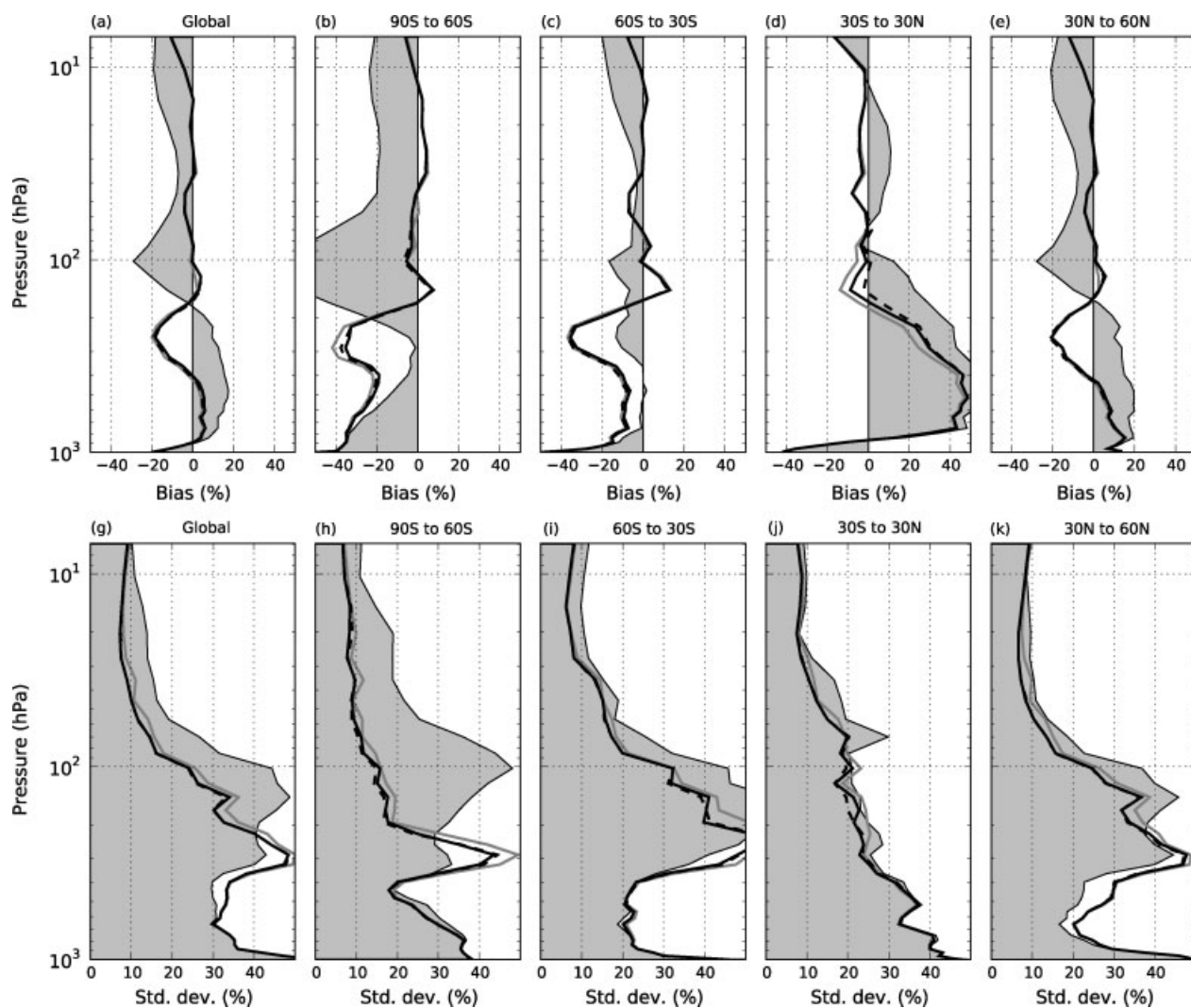


Figure 9. Same as Figure 8 but for differences with the ozonesondes.

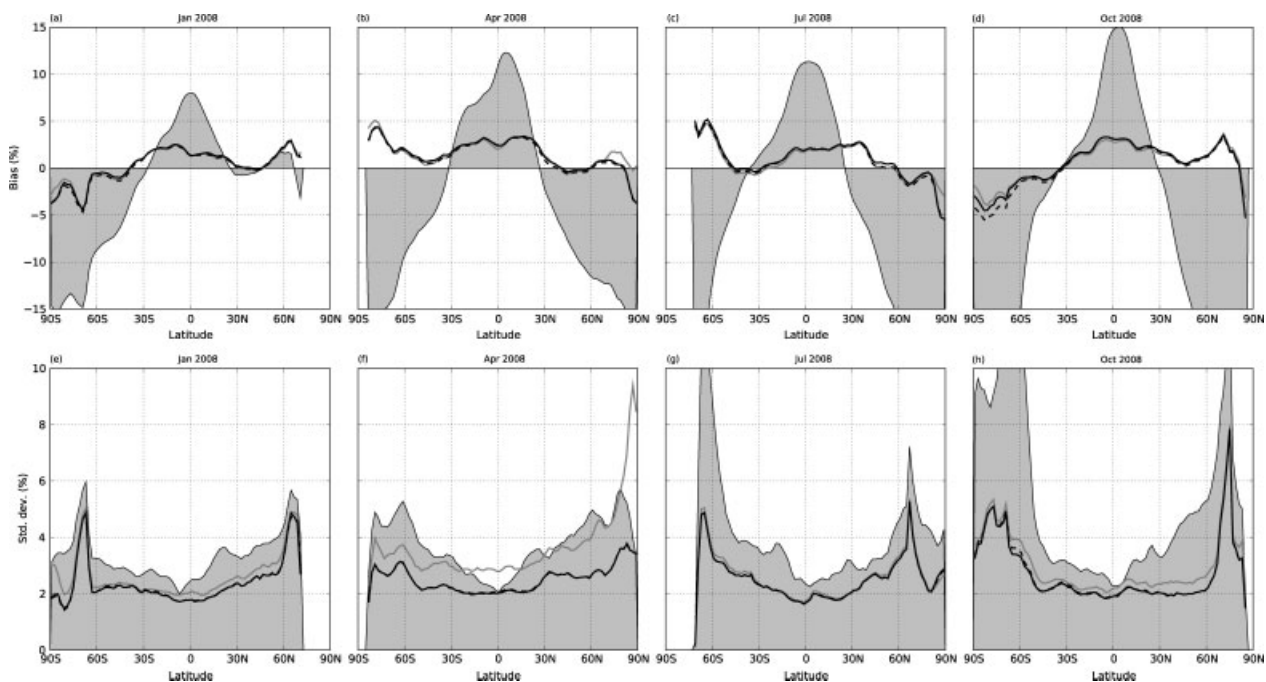


Figure 10. Mean (top) and standard deviation (bottom) of the difference (%) between OMI data and RAW model or analyses as a function of latitude, for January, April, July and October. For the top panel, positive (negative) values stand for an underestimation (overestimation) of the RAW model or the analyses compared to OMI data. See Table 1 for colour legend.

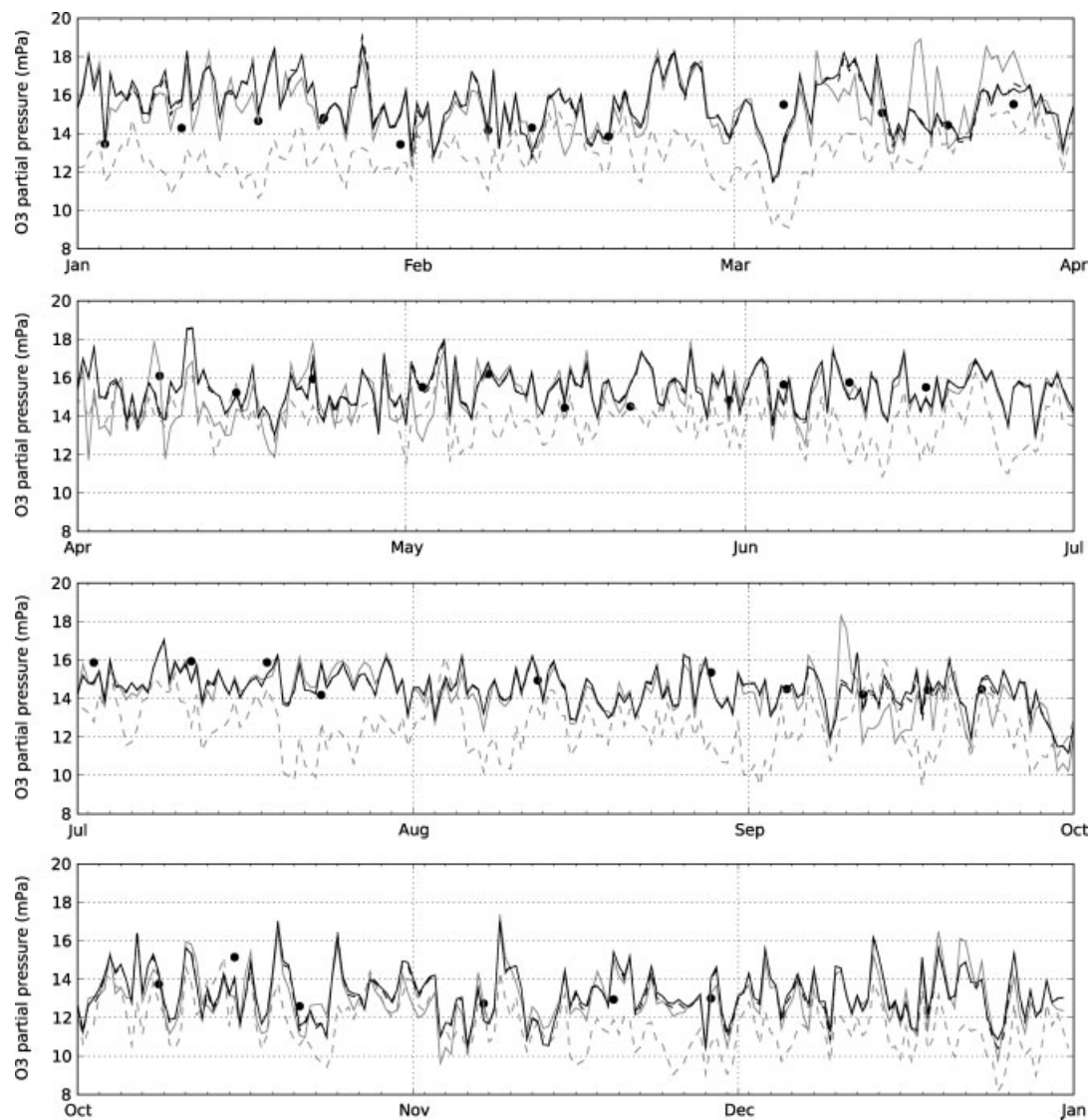


Figure 11. Ozone time series (mPa) at 20 hPa over the Maxaranguape (Natal) station (35.3°W , 5.5°S) from measurements (black dots) and from simulations (see Table I for colour legend, the RAW simulation being denoted by a dashed grey line here).

analysis STD reaches a few percent for all regions, while for the RAW simulation the STD is globally between 10% and 20%. When compared to ozonesondes, the stratospheric analysis STD is globally under 10%, while the RAW simulation STD ranges between 10% and 20% (Figure 9).

The observation error is higher over the UTLS region than the observation error found in the stratosphere (Figure 1). This acts to damp the data constraint on the analysis. As a consequence, the FULL analysis remains close to the RAW simulation and underestimates the ozone concentrations compared to MLS data, especially over the equatorial UTLS region (Figure 8). Nevertheless, compared to ozonesondes, the FULL analysis has a lower bias than the RAW simulation one over the equatorial region, in the UTLS and above (Figure 9). At highest latitudes, however, the FULL analysis produces concentrations of ozone that are too low compared to ozonesondes, leading to, for example, a bias of near 40% over the SPR between 200 and 300 hPa. Thus the assimilation of the MLS data does not allow reduction of the bias compared to ozonesondes below 215 hPa (localization of the MLS lowest measurement level), except in the equatorial region. Also, it does not allow reduction of the UTLS STD either (Figure 9). Sometimes, it may even amplify the STD.

For example, while the RAW simulation produces ozone concentrations with an averaged STD of 32% compared to ozonesondes, at 290 hPa in the 60°S to 90°S latitude band, the FULL analysis has a STD of nearly 44%.

The tropospheric bias of the FULL analysis compared to ozonesondes explains the bias of a few percent compared to OMI data, and observed in Figure 10, on the computed total ozone columns from the FULL analysis. Over the year, these columns are lower than those from OMI over the equatorial region. However, the bias is under 3%, while the columns obtained in the RAW simulation may have a bias over 10%. At the highest latitudes, the bias from the FULL analysis is still of the same order. However, the sign of the bias varies from one month to another, which has to be carefully interpreted as the number of measurements used to compute the statistics also have a seasonal variation (Figure 7).

Assimilating the MLS data allows considerable reduction, mostly at high latitudes, of the STD on the total ozone columns with respect to the OMI data, when compared to the RAW simulation. Figure 10 illustrates that at the highest latitudes the RAW simulation STD presents a seasonal variation, with its highest values found over the SPR, mainly

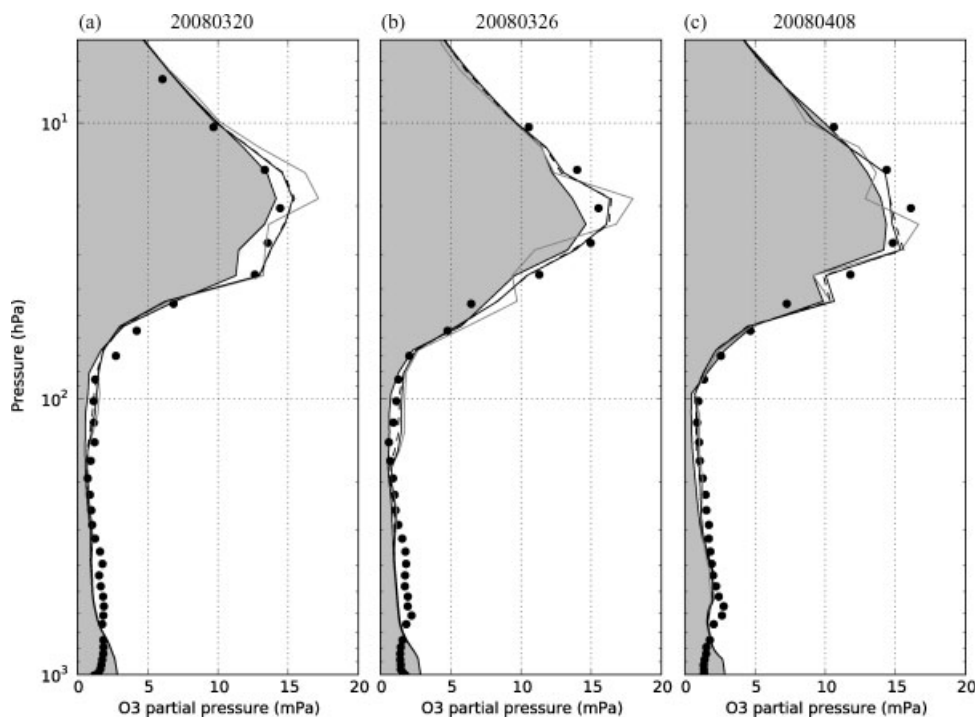


Figure 12. Ozone profiles (mPa) over the Maxaranguape (Natal) station (35.3°W, 5.5°S) from measurements (black dots) and from simulations (see Table I for colour legend) for three different dates: (a) 10 March, (b) 26 March and (c) 8 April 2008.

from June to December, with values which frequently are bigger than 12%. Meanwhile, the FULL analysis STD is approximately 2% except for locations that seem correlated to the vicinity of the polar vortex edges, where the STD grows to approximately 5%.

4.4. Evaluation of the PARTIAL experiment

The PARTIAL experiment is equivalent to the FULL experiment in the stratosphere, in terms of bias and STD, compared to MLS data and ozonesondes (Figures 8 and 9). The stratospheric standard deviation of the background error used in the PARTIAL experiment is, however, higher than that used for the FULL experiment (15% against 6–9%). Increasing the background error without significantly modifying the analysis means again that the low stratospheric observation error (compared to Σ) strongly constrains the analysis to be close to the observation. When the observation error increases in the mesosphere or in the UTLS, Σ begins to play a role. As in the mesosphere, Σ has lower values for the FULL experiment than for the PARTIAL one, the PARTIAL analysis is closer to the observations, while the FULL analysis is closer to the RAW simulation (Figure 8).

In the UTLS, the standard deviation of the background error in the PARTIAL experiment is, on the contrary, lower than that from the FULL experiment with values always over 15%, especially in the equatorial region. As a consequence, the PARTIAL analysis is closer to the RAW simulation, while the FULL analysis is closer to the MLS observations (Figure 8(d)). Also, when compared to ozonesondes, the two experiments are nearly statistically equivalent, but the PARTIAL analysis is always slightly better than the FULL one over the equatorial UTLS both in terms of bias and STD (Figure 9(d,j)). The only difference between the experiments is that the standard deviation of the background error is generally higher in the FULL experiment than in the PARTIAL

one. The PARTIAL experiment being here better than the FULL one would mean that the standard deviation of the background error is too high in the FULL experiment. As this comes from the ensemble-based estimation, it suggests that the estimated standard deviation of the background error is too high in the equatorial UTLS.

Nevertheless, over the SPR in October, the bias and the STD compared to OMI data are higher for the columns computed from the PARTIAL analysis than for those computed from the FULL analysis (Figure 10(d, h)). However, in this region, the ozone concentrations can have very low values during the formation of the ozone hole. As Σ is expressed as a percentage of the ozone concentration, it can have very low values. The experiment thus gives more confidence to the forecast.

4.5. Evaluation of the BASIC experiment

Compared to the MLS data, the BASIC experiment is statistically similar to the PARTIAL experiment over the stratosphere and the mesosphere (Figure 8). There are, however, few differences in the mesosphere over the SPR and the NPR where the BASIC analysis is closer to the observations (Figure 8(b, f)), but, compared to ozonesondes, the stratospheric STD is always slightly higher for this BASIC experiment than for the two previous experiments and for all latitude bands (Figure 9). Still comparing to ozonesondes, the STD is also slightly higher in the UTLS. This already shows that using constant length-scale for modelling the horizontal correlations of the background error has a negative impact on the analysis.

In terms of ozone total columns, the BASIC experiment has similar bias to the two other experiments in the major part of the domain. The differences are localized in the NPR and the SPR without any clear signal of improvement or deterioration as the signal varies from one month to another

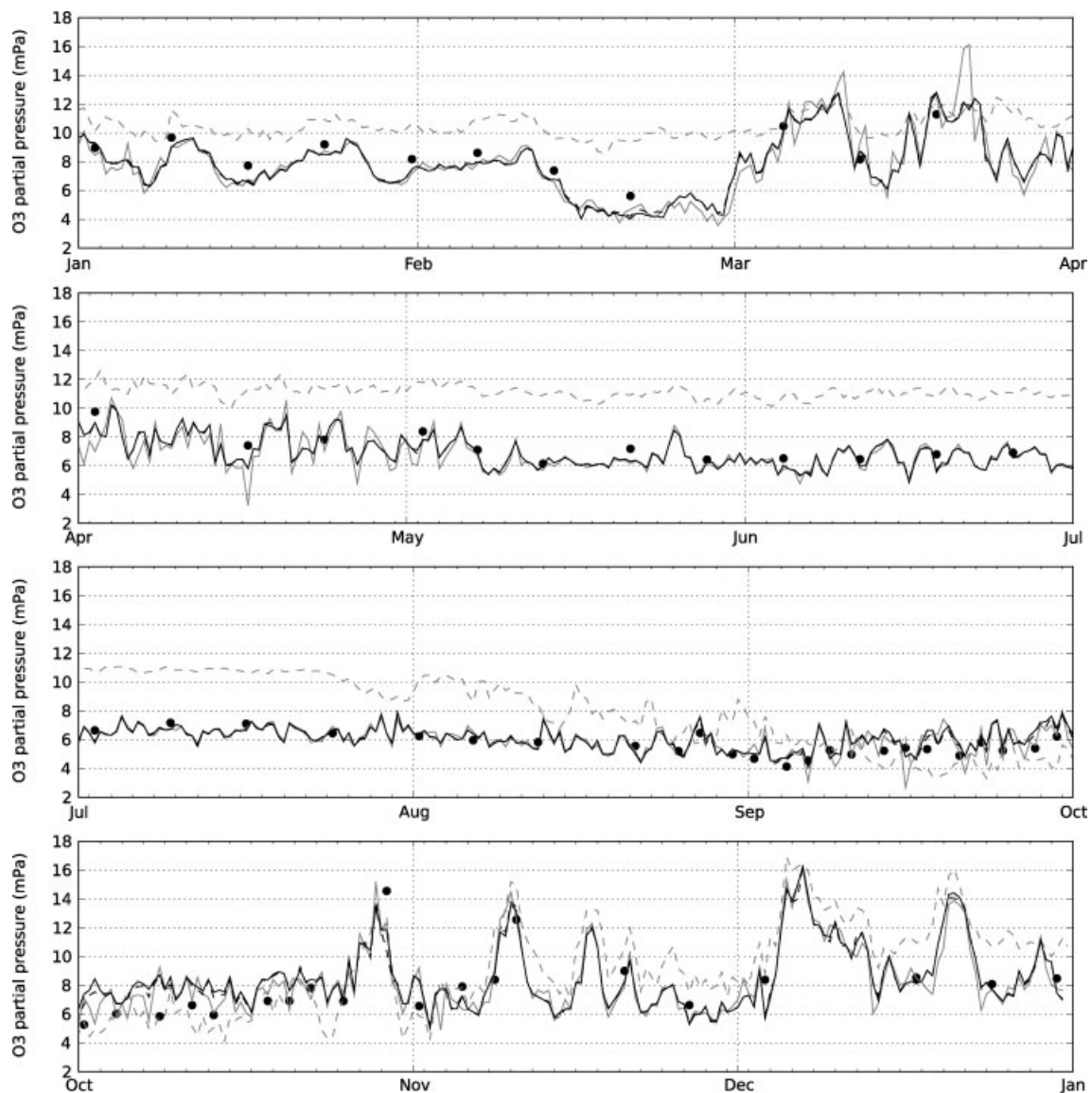


Figure 13. Ozone time series (mPa) at 20 hPa over the Neumayer station (8.3°W , 70.7°S) from measurements (black dots) and from simulations (see Table I for colour legend, the RAW simulation being denoted by a dashed grey line here).

(Figure 10). However, the BASIC experiment is characterized by higher STD than the other experiments. In particular, its STD over the equatorial region is even higher than that from the RAW simulation for April (Figure 10(f)). This is also illustrated by Figure 11, which presents the time evolution of the ozone concentration at 20 hPa over the Maxaranguape (Natal) station (35.3°W , 5.5°S) from the measurements and from the assimilation experiments. The analyses from all the experiments are similar to each other most of the time, and they are closer to the measurements than the RAW simulation. However, from the beginning of March to the middle of April, the ozone concentration from the BASIC analysis seems to have too much variability from one day to another. Figure 12 confirms that for this period the BASIC analysis produces stratospheric ozone profiles that may have high vertical variations, while the profiles from the measurements or from the other experiments are more smooth. Also, the stratospheric profiles from the BASIC analysis can noticeably vary from one date to another. A similar behaviour can be observed in the SPR at the same altitude, over the Neumayer station (8.3°W , 70.7°S ;

Figure 13), but for this station the BASIC analysis also differs from the other analyses in September and October.

As the PARTIAL experiment gives similar results to the FULL one, the observed inappropriate behaviour of the BASIC experiment comes exclusively from the choice of a constant length-scale to model the horizontal correlations of the background error.

5. Summary and discussion

The background error covariance matrix is known to be an important part of any assimilation system. It has to represent the uncertainties regarding the background state. It also has to represent the spatial correlation between these uncertainties and the correlation between the different variables of the model. As our assimilation system works with only one variable, i.e. the 3D ozone state, the paper is focused on the background uncertainties and their spatial correlations. These correlations are reduced to length-scales, which are the required parameters to represent them.

The first part of the paper estimated the statistics of the ozone background error with an ensemble of MLS data

assimilation. An ensemble of five members has allowed estimation of monthly statistics based on approximately 300 realizations. The BECM estimation showed variations of the statistics from one month to another. It allowed us to detect that the largest values of the background error standard deviation are located in the UTLS. Moreover, the background error correlations have larger length-scales in the zonal direction in the equatorial region, whereas they are more isotropic over the polar regions.

After estimating the background error statistics, we studied the impact of these estimations on the analysis by comparison with the assimilated data and independent data (profiles from ozonesondes and total ozone columns from OMI). The comparisons showed that the analysis using all the components of the estimated BECM produces ozone concentrations with a low bias and σ_{BD} , from the UTLS to the stratosphere.

Estimating the BECM has an important cost that could become unaffordable. We therefore tried to use simpler methods to calculate the BECM. Replacing the estimated standard deviation by a standard deviation proportional to the background value is one of them. This simplification does not significantly modify the analysis quality. Replacing the estimated length-scales with a constant value is the second simplification we tried. This dramatically deteriorated the analysis quality mainly from the beginning of March to the middle of April and in September and October. This simplification thus ought not to be applied to the analysis of stratospheric or tropospheric ozone. However, this has to be further investigated for the troposphere as our ensemble is obtained only by perturbing the MLS observations that have a lowest measurement at 215 hPa, which means that the tropospheric BECM estimations (in particular the length-scales) may be not so relevant. To bypass this, in the future we will have to build our ensemble using an ensemble of dynamical forcings. Also, we will also have to build it assimilating total columns or tropospheric measurements like those derived from the Infrared Atmospheric Sounding Interferometer (IASI) retrievals.

Notwithstanding this, even if the ensemble approach produces pertinent statistics of the BECM, it is extremely costly. Even using the simpler methods in trying to calculate the BECM is not a viable solution. We therefore plan to find a way to estimate this matrix on-line. An interesting approach would be to parametrize the covariance matrix with other physical parameters, as Elbern *et al.* (2010) did for the potential vorticity.

Acknowledgements

The development of the Valentina assimilation system has benefited from the support of the Ether Centre for Atmospheric Chemistry Products and Services <http://ether.ipsl.jussieu.fr>, and the French ADOMOCA project within the LEFE programs.

References

- Balis D, Kroon M, Koukouli ME, Brinksma EJ, Labow G, Veefkind JP, McPeters RD. 2007. Validation of Ozone Monitoring Instrument total ozone column measurements using Brewer and Dobson spectrophotometer ground-based observations. *J. Geophys. Res.* **112**: 1–10.
- Bannister RN. 2008a. A review of forecast error covariance statistics in atmospheric variational data assimilation. I: Characteristics and measurements of forecast error covariances. *Q. J. R. Meteorol. Soc.* **134**: 1951–1970.
- Bannister RN. 2008b. A review of forecast error covariance statistics in atmospheric variational data assimilation. II: Modelling the forecast error covariance statistics. *Q. J. R. Meteorol. Soc.* **134**: 1971–1996.
- Belo Pereira M, Berre L. 2006. The use of an ensemble approach to study the background error covariances in a global NWP model. *Mon. Weather Rev.* **134**: 2466–2489.
- Bousserez N, Attié JL, Peuch VH, Michou M, Pfister G, Edwards D, Emmons L, Mari C, Barret B, Arnold SR, Heckel A, Richter A, Schlager H, Lewis A, Avery M, Sachse G, Browell EV, Hair JW. 2007. Evaluation of the MOCAGE chemistry transport model during the ICARTT/ITOP experiment. *J. Geophys. Res.* **112**: D10S42, DOI: 10.1029/2006JD007595.
- Buehner M. 2005. Ensemble-derived stationary and flow-dependent background-error covariances: evaluation in a quasi-operational NWP setting. *Q. J. R. Meteorol. Soc.* **131**: 1013–1043.
- Cariolle D, Teyssède H. 2007. A revised linear ozone photochemistry parameterization for use in transport and general circulation models: multi-annual simulations. *Atmos. Chem. Phys.* **7**: 2183–2196.
- Claeyman M, Attié JL, El Amraoui L, Cariolle D, Peuch VH, Teyssède H, Josse B, Ricaud P, Massart S, Piacentini A, Cammas JP, Livesey NJ, Pumphrey H, Edwards DP. 2010. A linear CO chemistry parameterization in a chemistry-transport model: evaluation and application to data assimilation. *Atmos. Chem. Phys.* **10**: 6097–6115.
- Daley R. 1991. *Atmospheric Data Analysis*. Cambridge Atmospheric and Space Sciences Series. Cambridge University Press: Cambridge, UK.
- Dufour A, Amodei M, Ancellet G, Peuch VH. 2004. Observed and modelled 'chemical weather' during ESCOMPTE. *Atmos. Res.* **74**: 161–189.
- El Amraoui L, Attié JL, Semane N, Claeyman M, Peuch VH, Warner J, Ricaud P, Cammas JP, Piacentini A, Josse B, Cariolle D, Massart S, Bencherif H. 2010. Midlatitude stratosphere–troposphere exchange as diagnosed by MLS O₃ and MOPITT CO assimilated fields. *Atmos. Chem. Phys.* **10**: 2175–2194.
- Elbern H, Schwinger J, Botchorishvili R. 2010. Chemical state estimation for the middle atmosphere by four-dimensional variational data assimilation: system configuration. *J. Geophys. Res.* **115**: D06302, DOI: 10.1029/2009JD011953.
- Fortuin JPF, Kelder H. 1998. An ozone climatology based on ozonesonde and satellite measurements. *J. Geophys. Res.* **103**: 709–734.
- Froidevaux L, Jiang YB, Lambert A, Livesey NJ, Read WG, Waters JW, Browell EV, Hair JW, Avery MA, McGee TJ, Twigg LW, Summnick GK, Jucks KW, Margitan JJ, Sen B, Stachnik RA, Toon GC, Bernath PF, Boone CD, Walker KA, Filipiak MJ, Harwood RS, Fuller RA, Manney GL, Schwartz MJ, Daffer WH, Drouin BJ, Cofield RE, Cuddy DT, Jarnot RF, Knosp BW, Perun VS, Snyder WV, Stek PC, Thurstans RP, Wagner PA. 2008. Validation of Aura Microwave Limb Sounder stratospheric ozone measurements. *J. Geophys. Res.* **113**: D15S20, DOI: 10.1029/2007JD008771.
- Geer A, Lahoz W, Bekki S, Bormann N, Errera Q, Eskes H, Fonteyn D, Jackson D, Juckes M, Massart S, Peuch VH, Rharmili S, Segers A. 2006. The ASSET intercomparison of ozone analyses: method and first results. *Atmos. Chem. Phys.* **6**: 5445–5474.
- Kalnay E. 2003. *Atmospheric Modeling, Data Assimilation and Predictability*. Cambridge University Press: Cambridge, UK.
- Lahoz WA, Geer AJ, Bekki S, Bormann N, Ceccherini S, Elbern H, Errera Q, Eskes HJ, Fonteyn D, Jackson DR, Khattatov B, Massart S, Peuch VH, Rharmili S, Ridolfi M, Segers A, Talagrand O, Thornton HE, Vik AF, von Clarmann T. 2007. The assimilation of envisat data (ASSET) project. *Atmos. Chem. Phys.* **7**: 1773–1796.
- Levelt PF, van den Oord GHJ, Dobber MR, Malkki A, Visser H, de Vries J, Stammes P, Lundell JOV, Saari H. 2008. The Ozone Monitoring Instrument. *Geosci. Remote Sens.* **44**: 1093–1101.
- Livesey NJ, Filipiak MJ, Froidevaux L, Read WG, Lambert A, Santee ML, Jiang JH, Pumphrey HC, Waters JW, Cofield RE, Cuddy DT, Daffer WH, Drouin BJ, Fuller RA, Jarnot RF, Jiang YB, Knosp BW, Li QB, Perun VS, Schwartz MJ, Snyder WV, Stek PC, Thurstans RP, Wagner PA, Avery M, Browell EV, Cammas JP, Christensen LE, Diskin GS, Gao RS, Jost HJ, Loewenstein M, Lopez JD, Nedelec P, Osterman GB, Sachse GW, Webster CR. 2008. Validation of Aura Microwave Limb Sounder O₃ and CO observations in the upper troposphere and lower stratosphere. *J. Geophys. Res.* **113**: D15S02, DOI: 10.1029/2007JD008805.
- Logan JA. 1999. An analysis of ozonesonde data for the troposphere: recommendations for testing 3-D models and development of a gridded climatology for tropospheric ozone. *J. Geophys. Res.* **104**: 115–149.
- Lorenc AC. 2003. The potential of the ensemble Kalman filter for NWP: a comparison with 4D-Var. *Q. J. R. Meteorol. Soc.* **129**: 3183–3203.

- Massart S, Piacentini A, Cariolle D, El Amraoui L, Semane N. 2007. Assessment of the quality of the ozone measurements from the Odin/SMR instrument using data assimilation. *Can. J. Phys.* **85**: 1209–1223.
- Massart S, Clerbaux C, Cariolle D, Piacentini A, Turquety S, Hadji-Lazaro J. 2009. First steps towards the assimilation of IASI ozone data into the MOCAGE-PALM system. *Atmos. Chem. Phys.* **9**: 5073–5091.
- Massart S, Pajot B, Piacentini A, Pannekoucke O. 2010. On the merits of using a 3D-FGAT assimilation scheme with an outer loop for atmospheric situations governed by transport. *Mon. Weather Rev.* **138**: 4509–4522.
- Mirouze I, Weaver AT. 2010. Representation of correlation functions in variational assimilation using an implicit diffusion operator. *Q. J. R. Meteorol. Soc.* **136**: 1421–1443.
- Pannekoucke O, Massart S. 2008. Estimation of the local diffusion tensor and normalization for heterogeneous correlation modelling using a diffusion equation. *Q. J. R. Meteorol. Soc.* **134**: 1425–1438.
- Pannekoucke O, Berre L, Desroziers G. 2008. Background-error correlation length-scale estimates and their sampling statistics. *Q. J. R. Meteorol. Soc.* **134**: 497–508.
- Peuch VH, Amodei M, Barthet T, Cathala ML, Michou M, Simon P. 1999. MOCAGE, MOdèle de Chimie Atmosphérique à Grande Echelle. In *Proceedings of Météo France: Workshop on Atmospheric Modelling*. Toulouse, France; 33–36.
- Schwinger J, Elbern H. 2010. Chemical state estimation for the middle atmosphere by four-dimensional variational data assimilation: a posteriori validation of error statistics in observation space. *J. Geophys. Res.* **115**: D18307, DOI: 10.1029/2009JD013115.
- Semane N, Peuch VH, Pradier S, Desroziers G, El Amraoui L, Brousseau P, Massart S, Chapnik B, Peuch A. 2009. On the extraction of wind information from the assimilation of ozone profiles in Météo-France 4D-Var operational NWP suite. *Atmos. Chem. Phys.* **9**: 4855–4867.
- Smit HGJ, Strater W, Helten M, Kley D, Ciupa D, Claude HJ, Kohler U, Hoegger B, Levrat G, Johnson B, Oltmans SJ, Kerr JB, Tarasick DW, Davies J, Shitamichi M, Srivastav SK, Vialle C, Velghe G. 1998. JOSIE: The 1996 WMO International intercomparison of ozonesondes under quasi flight conditions in the environmental simulation chamber at Jülich. In *Proceedings of the XVIII Quadrennial Ozone Symposium*, L'Aquila, Italy, September 1996; 971–974.
- Talagrand O. 2003. Objective validation and evaluation of data assimilation. In *Proceedings of Seminar on Recent Developments in Data Assimilation for Atmosphere and Ocean*, ECMWF, Reading; 287–299.
- Teyssède H, Michou M, Clark HL, Josse B, Karcher F, Ollivier D, Peuch VH, Saint-Martin D, Cariolle D, Attié JL, Nédélec P, Ricaud P, Thouret V, van der A RJ, Volz-Thomas A, Chéroux F. 2007. A new tropospheric and stratospheric Chemistry and Transport Model MOCAGE-Climat for multi-year studies: evaluation of the present-day climatology and sensitivity to surface processes. *Atmos. Chem. Phys.* **7**: 5815–5860.
- Veefkind JP, de Haan JF, Brinksma EJ, Kroon M, Levelt PF. 2006. Total ozone from the Ozone Monitoring Instrument (OMI) using the DOAS technique. *Geosci. Remote Sens.* **44**: 1239–1244.
- Waters JW, Froidevaux L, Harwood RS, Jarnot RF, Pickett HM, Read WG, Siegel PH, Cofield RE, Filipiak MJ, Flower DA, Holden JR, Lau GK, Livesey NJ, Manney GL, Pumphrey HC, Santee ML, Wu DL, Cuddy DT, Lay RR, Loo MS, Perun VS, Schwartz MJ, Stek PC, Thurstans RP, Boyles MA, Chandra KM, Chavez MC, Chen GS, Chudasama BV, Dodge R, Fuller RA, Girard MA, Jiang JH, Jiang Y, Knosp BW, LaBelle RC, Lam JC, Lee KA, Miller D, Oswald JE, Patel NC, Pukala DM, Quintero O, Scaff DM, Van Snyder W, Tope MC, Wagner PA, Walch MJ. 2006. The Earth Observing System Microwave Limb Sounder (EOS MLS) on the Aura satellite. *IEEE Trans. Geosci. Remote Sens.* **44**: 1075–1092.
- Weaver A, Courtier P. 2001. Correlation modelling on the sphere using a generalized diffusion equation. *Q. J. R. Meteorol. Soc.* **127**: 1815–1846.